Acta Oceanol. Sin., 2011, Vol. 30, No. 5, P. 56-63
DOI: 10.1007/s13131-011-0147-y
http://www.hyxb.org.cn
E-mail: hyxbe@263.net

Winter heat budget in the Huanghai Sea and the effect from Huanghai Warm Current (Yellow Sea Warm Current)

QIAO Lulu[1,2,3*], WANG Xiaohua[3,4], WANG Yongzhi[5], WU Dexing[2], BAO Xianwen[2], MU Lin[6]

[1] Key Laboratory of Seafloor Science and Exploration Technology, Ocean University of China, Qingdao 266100, China

[2] Key Laboratory of Physical Oceanography, Ministry of Education, Ocean University of China, Qingdao 266100, China

[3] School of Physical, Environmental and Mathematical Sciences, University of New South Wales at Australian Defence Force Academy, Canberra, Australia

[4] State Key Laboratory of Satellite Ocean Environment Dynamics, Second Institute Oceanography, State Oceanic Administratim, Hangzhou 310012, China

[5] The First Institute of Oceanography, State Oceanic Administration, Qingdao 266061, China

[6] National Marine Data and Information Service, State Oceanic Administration, Tianjin 300171, China

Received 4 January 2011; accepted 14 June 2011

©The Chinese Society of Oceanography and Springer-Verlag Berlin Heidelberg 2011

Abstract
Four sources of surface heat flux (SHF) and the satellite remote sensing sea surface temperature (SST) data are combined to investigate the heat budget closure of the Huanghai Sea (HS) in winter. It is found that heat loss occurs all over the HS during winter and the area averaged heat content change decreases with a rate of –106 W/m^2. Comparing with the area averaged SHF of –150 W/m^{-2} from the four SHF data sets, it can be concluded that the SHF plays a dominant role in the HS heat budget during winter. In contrast, the heat advection transported by the Huanghai Warm Current (Yellow Sea Warm Current, HWC) accounted for up to 29% of the HS heat content change. Close correlation, especially in February, between the storm events and the SST increase demonstrates that the HWC behaves strongly as a wind-driven compensation current.

Key words: heat budget, Huanghai Sea and Bohai Sea, surface heat flux, Huanghai Warm Current (Yellow Sea Warm Current)

1 Introduction

The Huanghai Sea (Yellow Sea, HS), a typical continental shallow sea, is located between China and the Korean Peninsula. To the north it penetrates to the Bohai Sea (BS) and connects to the East China Sea (ECS) to the south with a boundary line joining Qidong and Jeju Island (Fig. 1). Water depth in the HS is characterized by a deep trough distributing from southeast to north, with a depth around 80 m (Fig. 1). In this work, our study of the HS includes both HS and BS.

One of the most important currents in the HS is the Huanghai Warm Current (Yellow Sea Warm Current, HWC, see Fig. 1) which brings warm and saline water into the HS. Uda (1936) first described the HWC as a branch of the Tsushima Warm Current. His work was followed by Nitani (1972) and Guan (1994). In contrast, Hsueh et al. (1986) considered the HWC as a compensatory current due to winter northerly wind. Later analyses and numerical studies further confirmed this conclusion (Liu, 1996; Guo et al., 2000;

Foundation item: The National Natural Science Foundation Project "Sedimentary dynamic mechanism of the Huanghai Warm Current" of China under contract No.40906025; the State Basic Research Program of China under contract No. 2010CB428704; the National Natural Science Foundation of China " The process and mechanism of the increasing of surface temperature in the past 30 years in the adjacent seas of China" under contract No. 40930844; the Formation and development of the muddy deposition in the central southern Huanghai Sea, and its relation with climate and environmental change of Ocean University of China under contract No.41030856; the Scientific Research Fund of the Second Institute of Oceanography, State Oceanic Administration of China under contract No. JT1007; the Public Science and Technology Research Funds Projects of Ocean under contract Nos 200905001 and 201005019; the National Natural Science Foundation of China under contract No.41006002.
*Corresponding author, E-mail: qiaolulu126@sina.com

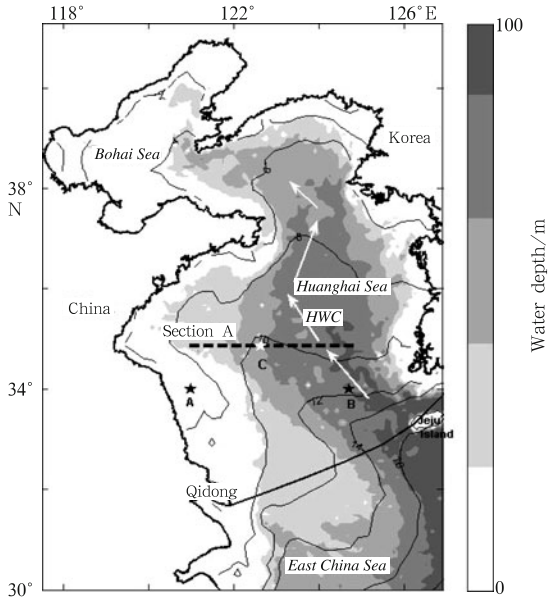

Fig.1. Water depth (filled color) and AVHRR climatological winter-averaged SST (°C, solid contour lines) in the HS. White arrows show the path of the HWC in the HS. Dash black line denotes Section A. Two black starts mark two stations in the shallow water (at 34°N, 121°E) and warm tongue area (at 34°N, 124.7°E) of the HS, respectively. White star (at 34.85°N, 122.625°E) in Section A marks Station C.

Teague and Jacobs, 2000; Zang et al., 2001). From the numerical simulation, Liu (1996) concluded that both the HWC and southward coastal flows along Korean and Chinese coast were due to the combining effect of topography and northerly wind; Teague and Jacobs (2000) reported that the HWC was forced by a north-to-south pressure gradient caused by strong northerly wind bursts.

Despite the above advancement in the HWC study, the effect of the HWC on the winter heat budget in the HS is still poorly understood. Wang and Yuan (1988) suggested that the warm tongue in the HS in winter was most likely due to the rapidly cooling in shallow water but not related to the northward advection of heat. Xie et al. (2002) also suggested that the warm tongue was the effect of bathymetry with the intense surface cooling in winter. However, Riedlinger and Jacobs (2000) reported that the Kuroshio and the Taiwan Warm Current could intrude into the HS, advecting warm waters into the HS. Huang et al. (2005) pointed out that both surface cooling and advection of the current play an important role in the formation of the tongue in the winter. Ma et al. (2006) concluded that the bathymetric effect was a large contributor in forming the temperature gradient, while the HWC was also an important factor in determining the warm tongue's structure and position.

Thus in this paper we aim at studying the HS heat budget during wintertime and the role that of the HWC plays in the balance of this heat budget. The wintertime in this work is defined as December, January and February according to Chen et al. (1992).

2 Data

2.1 *Surface heat flux*

The available data source related to the SHF can be divided into four kinds: in-situ based fluxes, e.g., NOC1.1a which is a product from the National Oceanography Centre (NOC), Southampton enhanced with additional metadata from the International List of Selected, Supplementary and Auxiliary Ships (the WMO Report 47) (Josey et al., 1998); satellite-derived fluxes: the cloud and radiative fluxes from the International Satellite Cloud Climatology Project (ISCCP); numerical SHFs, such as the product of the European Centre for Medium Range Weather Forecasts (ECMWF) 40 a Re-analysis Project (ERA40) and the product of National Centers for Environmental Prediction Reanalysis (NCEPR); and the blended ones, for example, latent and sensible SHFs from the Objectively Analyzed Air-sea Fluxes (OAFlux) Project which is sponsored by the NOAA through the WHOI and net short wave and long wave radiation from the ISCCP (OAFlux/ISCCP) (Yu and Weller, 2008).

The climatological monthly mean data for the NOC1.1a are readily available. However, for the NCEPR and the ERA40 the climatology products were calculated by integrating data for the same time period as the NOC1.1a from 1980 to 1993, and for the OAFlux/ISCCP integrating from 1983 to 1993 because of data limitation. The detailed information of data sets can be found in Table 1. Considering the high quality of NOC1.1a which is based on the in-situ observations (Josey et al., 1998), evaluation and comparison of the other three data sets were conducted by using the NOC1.1a data as a benchmark.

The climatologic monthly area-averaged SHF of NOC1.1a with its differences with other data sources in the HS was shown in Fig. 2. The ERA40 supplies an overestimated solar radiation and net SHF in winter, while the other three components of SHF compare well with NOC1.1a. Net SHF with its sensible

component of OAFlux/ISCCP in winter is underestimated. Almost all the components and the net SHF itself in winter of NCEPR showed a smaller value than NOC1.1a except for solar radiation. Thus Figs 2b–d indicate that ERA40 appears to be better compared with NOC1.1a than OAFlux/ISCCP and NCEPR for the study in the HS in winter.

Table 1. Description of SHF and SST data

Data sources		Spatial resolution	Duration	Temporal resolution	Spatial range
SHF	NOC1.1a	1°×1°	1980–1993	climatological	84.5°S–84.5°N, 0°–359°E
	ERA40	1.125°×1.125°	1980–1993	6 h	89.1452°S–89.14152°N, 0°–358.875°E
	OAFlux/ISCCP	1°×1°	1983–1993	daily	64.5°S–64.5°N, 0.5°–359.5°E
	NCEPR	1.875°×1.905°	1980–1993	monthly	88.542°S–88.542°N, 0°–358.125°E
SST	AVHRR	4 km×4 km	1985–2005	climatologic monthly	89.98°S–89.98°N, 179.982°W–179.982°E
	TMI	0.25°×0.25°	1997–2008	daily	39.875°S–39.875°N, 0.125°–359.875°E

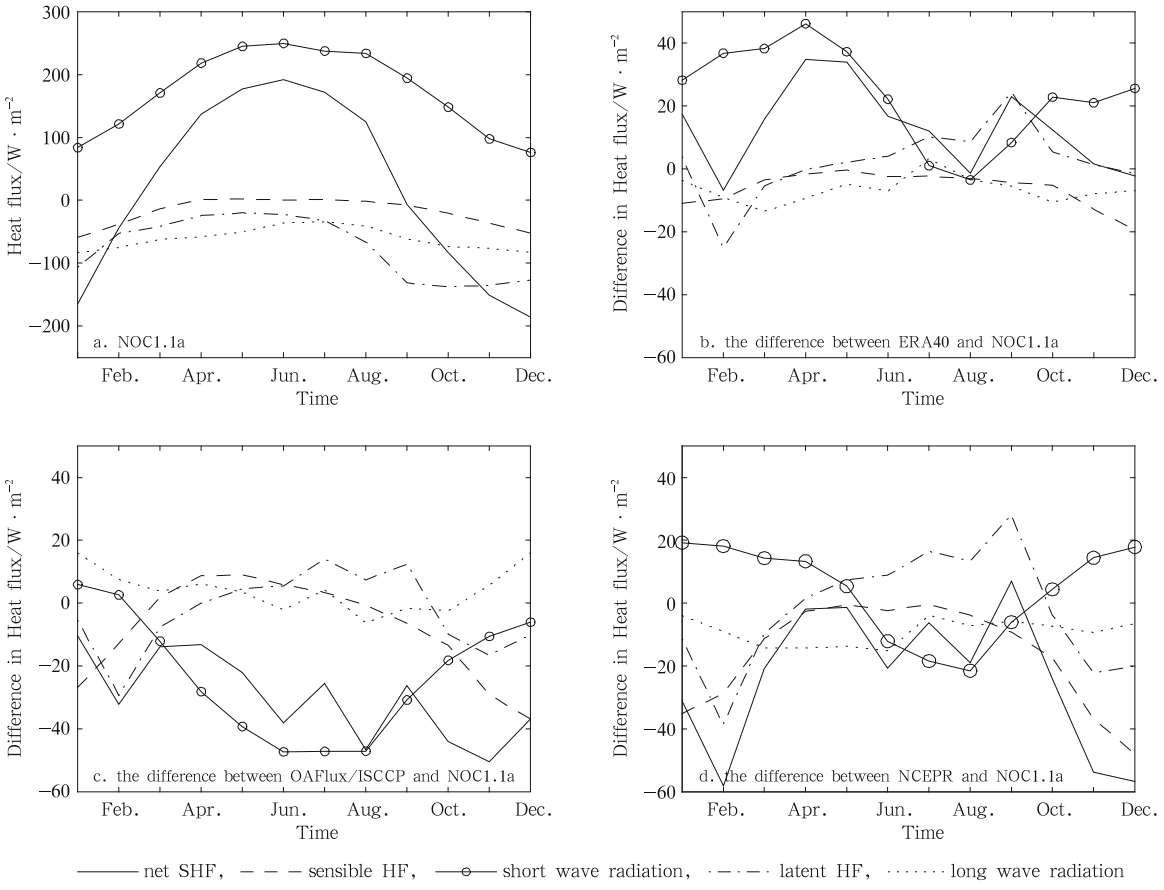

Fig.2. Climatological monthly area averaged net SHF with four components of NOC1.1a (a) in the HS and the difference between NOC1.1a and other three data sources (b–d).

2.2 *Sea surface temperature*

The climatologic monthly SST data come from the AVHRR (NOAA advanced very-high-resolution radiometer oceans) pathfinder, and are averaged from 1985 to 2005 (Table 1). As shown in Fig. 1, the warm tongue in the HS can be clearly observed in winter.

While the monthly AVHRR SST data have a high spatial resolution and are advantageous in analyzing the long-term variability, the frequent cloud cover prevents a better description of high frequency events such as the winter storms in the HS region. Thus another daily SST product from the TMI radiometer with a 10.7 GHz channel launched aboard the tropical rainfall measuring mission (TRMM) satellite was used. TRMM is a joint mission between the NASA and the Japan Aerospace Exploration Agency (JAXA). An important feature of this SST data set is the microwave

retrievals which can measure the SST through clouds and are neither affected by aerosols nor sensitive to atmospheric water vapor. Detailed description of this data set can be found in Table 1.

3 HS heat budget

3.1 *The HS SHF in winter*

The winter-averaged net SHFs of four data sources integrated from December to February were shown in Fig.3. During the winter season, the net SHF of all the HS is negative with an area-averaged value of –132 W/m^2 according to NOC1.1a and –129 W/m^2 based on ERA40, while the results calculated by OAFlux/ISCCP and NCEPR were biased low with a value of –158 and –180 W/m^2, respectively (Table 2). The contour lines of net SHF were in the longitudinal direction, and the largest surface cooling occurred in the southeast of the HS with a value of –273 W/m^2 according to NOC1.1a. The similar distributions were illustrated by other three data sources, although they showed larger surface cooling in the southeast of the HS. NCEPR also showed a smaller value in the north HS.

This horizontal distribution of net SHF from the above data sets is different from the work of Ma et al. (2006) which showed the largest negative net SHF in the central HS. Their calculation was made by using a simple atmospheric feedback scheme (Harney, 1971), though their results were integrated from October to

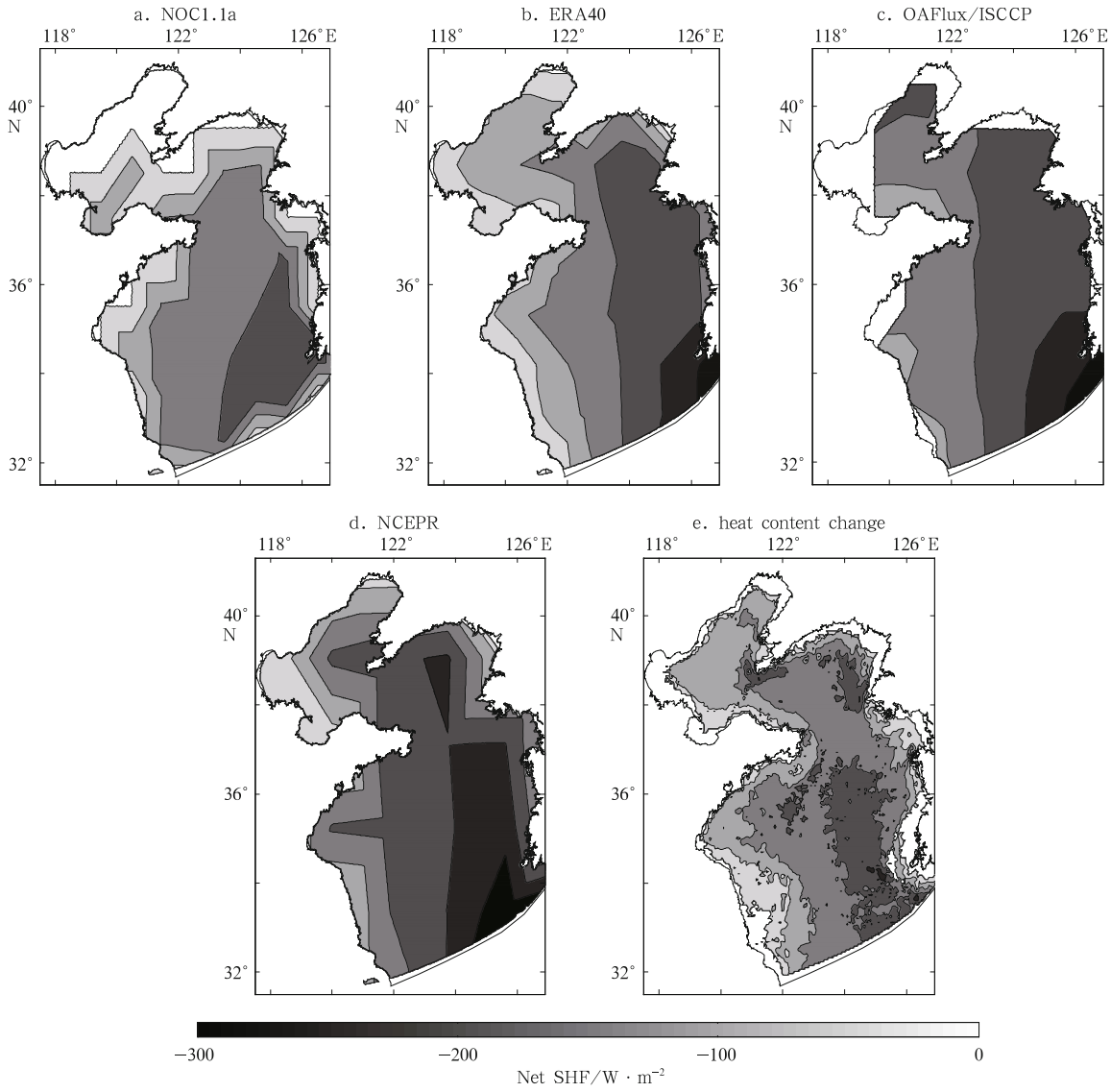

Fig.3. Time-averaged HS net SHF from NOC1.1a (a), ERA40 (b), OAFlux/ISCCP (c), NCEPR (d) and heat content change (e) during winter.

Table 2. Area-averaged net SHF (Q_{ne}) of four data sources, depth integrated heat content (Q_{hc}) change, and the heat advection ($Q_{ad} = Q_{hc} - Q_{ne}$) in the HS over winter. The average < > was calculated from four data sources. q_{ne} denotes the standard deviation of Q_{ne} from the average value (unit in W/m^2)

Q_{hc}		Q_{ne}	q_{ne}	Q_{ad}	1–Q_{hc}/Q_{ne}
–106	NOC1.1a	–132	18	26	20%
	ERA40	–129	21	23	18%
	OAFlux/ISCCP	–158	–8	52	33%
	NCEPR	–180	–30	74	41%
	< >	–150		44	29%

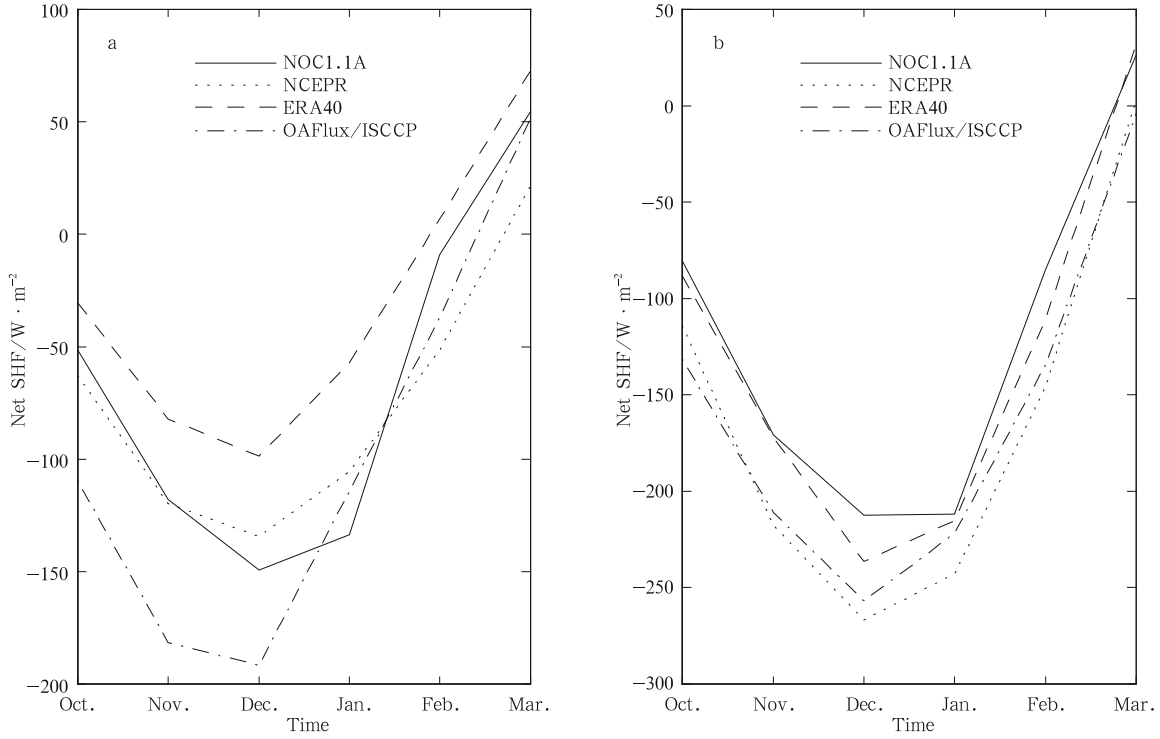

Fig.4. Net SHF at two locations marked in Fig. 1. a. Station A and b. Station B.

March. We note that the net SHF from NOC1.1a of the above period illustrated the same distribution as shown in Fig. 3a. Furthermore, their time series of net SHF at two locations, in the shallow water and warm tongue area of the HS, were again different to those obtained from the four data sets (Figs 4a, b). Although there were some minor differences in their minimum value, all data sources from this study exhibited the same trend in the net SHF variation in the shallow water and warm tongue area, with the largest surface cooling occurred in December. However, according to Ma et al. (2006), the lowest value in the shallow water described was in October (Fig. 13a in Ma et al., 2006), while in the warm tongue area, the net SHF reached a minimum value in January.

3.2 *The HS heat budget in winter*

Similar to Wang and Symonds (1999) and Wang (2005), the HS heat content change integrated over the depth can be estimated by $Q_{hc} = \int_{-H}^{0} \rho c \Delta T \mathrm{d}z$ where ρ is the water density; c is the specific heat capacity and equals to 3 980 J/(kg·K); and ΔT is the temperature change during the winter, where the monthly satellite SST data of AVHRR are used with the observed fact that the water of the HS is well mixed in winter due to strong wind mixing (Le and Mao, 1990).

During winter, heat loss occurred all over the HS (Fig. 3e), at an area-averaged rate of –106 W/m^2 (Table 2). The largest heat content change occurring near the HS trough can reach –244 W/m^2, partly because of the close relationship between the heat content change and the water depth. As comparing with the net SHF during winter, both the similar distribution and the approximate area-averaged value indicate that SHF has played a dominant role in the HS heat

content change during winter. The effect of heat advection on the HS heat budget in winter can be revealed by subtracting the net SHF Q_{ne} from the heat content change Q_{hc}. Using four data sets, an averaged value of 44 W/m^2 was transported into the HS by horizontal advection, and accounted for 29% of the HS heat content change in winter (Table 2). The extent of this effect due to advection is clearly determined by the strength of the HWC.

4 Discussion and conclusions

Storm event, a familiar synoptic phenomenon in winter of the HS, can last for several days with a strong northerly wind and a large decrease in the air temperature in an order of magnitude of 10 m/s and 10°C, respectively.

As shown in Fig. 5, the storm events from December 1997 to February 1998 occurred approximately every 5 d. These events were marked with strong wind stress and heat loss in excess of 0.2 N/m^2 and –500 W/m^2, respectively. In response to the heavy wind during each storm event (Figs 5a and b), the SST increased immediately against large surface cooling in the HWC region around 123°E along Section A (Fig. 5c). The correlation coefficient between the storm events and the temperature can reach a maximum of 0.75 in February. This close correlation (Figs 6a and b) demonstrated that the HWC behaves strongly as a wind-driven compensation current in response to the winter storm events. The water temperature increase was most likely a result of increased horizontal heat advection by a strengthened HWC in response to the strong northerly wind during the storm events.

To further support the above conclusion, we have conducted a numerical experiment simulating a barotropic HS in response to the winter storm events. The model used ECOMSED (Blumberg, 1996; Lick et al., 1995) and was forced by an ERA40 winter area-averaged northwesterly wind of 9 m/s for 90 d. For the details of the model experiment, refer to Qiao's (2008) PhD thesis. The model simulation shows a depth-averaged upwind flow in the deeper central HS where the north-south pressure gradient due to surface slope is greater than the wind stress; and southward currents

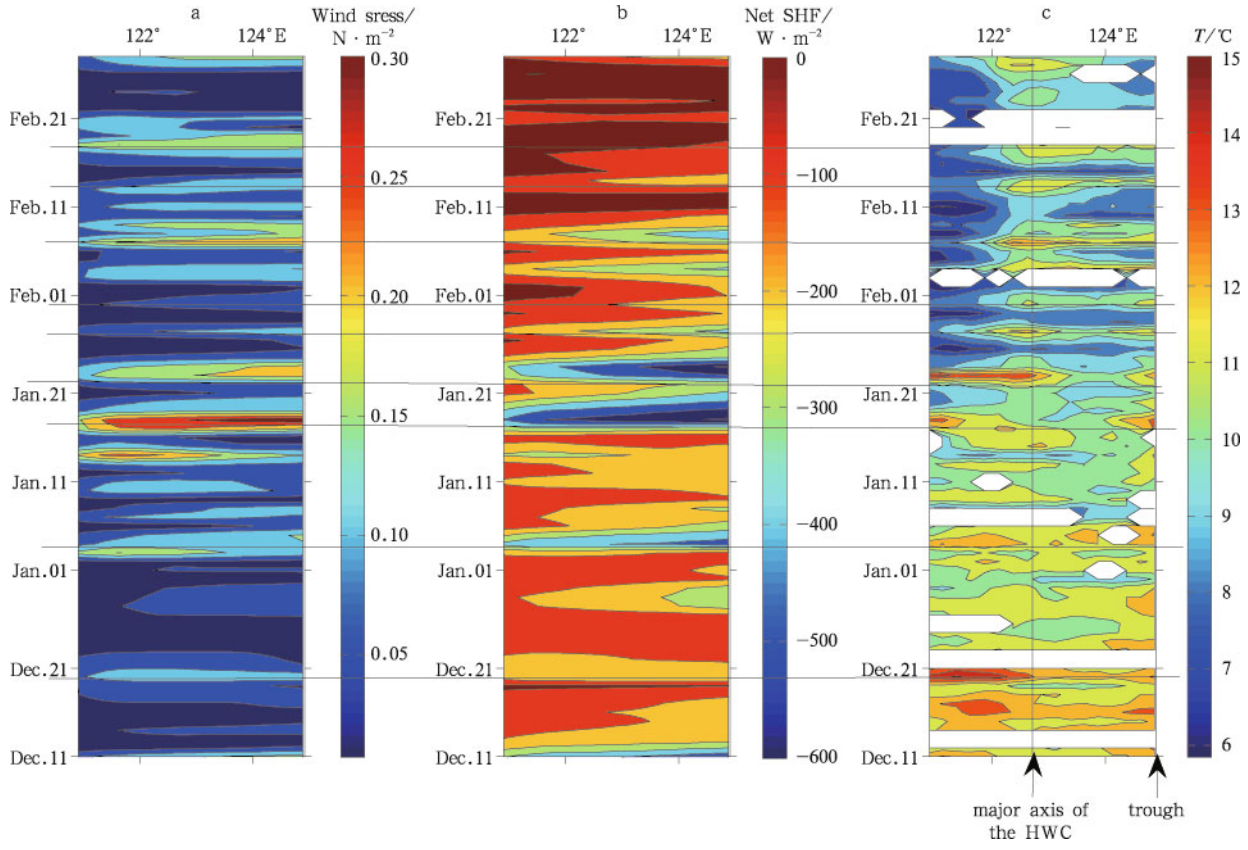

Fig.5. ERA40 6-h product of wind stress (a), net SHF (b) and TMI daily SST (c) in Section A during the winter of 1997–1998. Black lines in Fig. 5c illustrate the location of the major axis of the HWC.

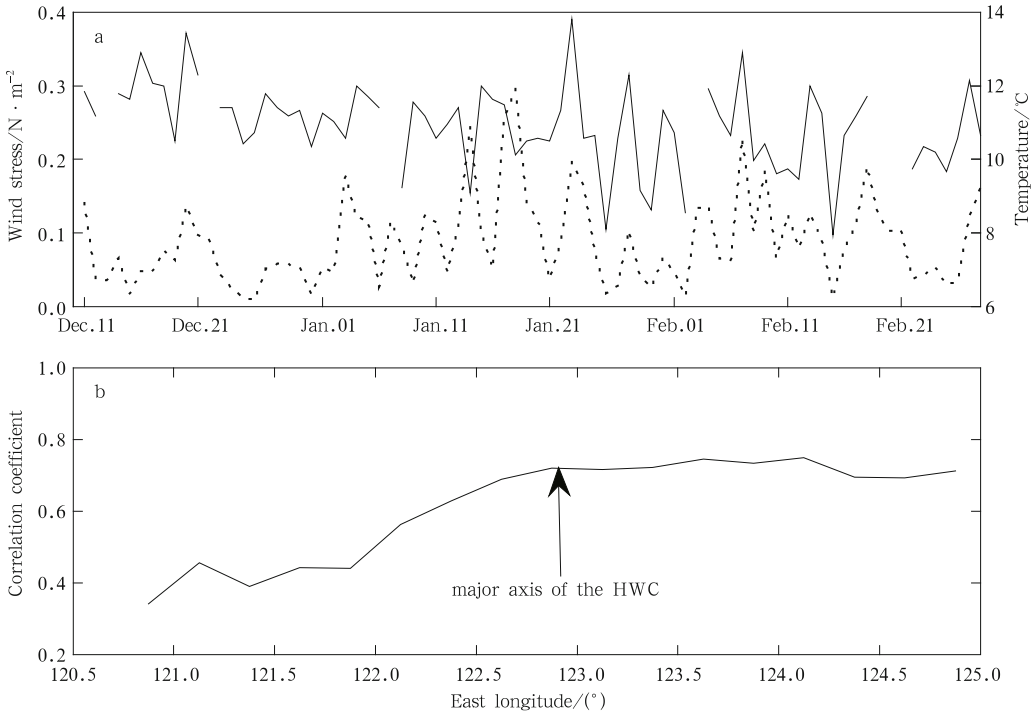

Fig.6. Time series of SST (solid line), wind stress (dashed line) (a) at Station C (marked in Fig. 1) and correlation coefficient between wind stress and SST in Section A (b) in February 1998.

flowing along the shallow Chinese and Korean coasts where the wind stress is greater than the pressure gradient (figure not shown). This model result agrees with Csanady (1981) who neglected effect of bottom friction and Coriolis force in his study of wind-driven current in a closed basin. Thus the HWC inflow can be explained as a wind-driven compensation current in response to the winter storm events.

It should be noted that large westward shifts of the major axis of the HWC can also be observed during some strong cold events (e.g., 17 and 23 January 1998, Fig. 5c). The cause of this shift has been discussed by previous authors (e.g., Tang et al., 2001; Huang et al., 2005), and is the subject of a separate study.

There was heat loss all over the HS during winter and the winter-averaged heat content change decreased at an area-averaged rate of –106 W/m^2. As comparing with the similar horizontal distribution and winter averaged value of SHF of –150 W/m^2 averaged from four data sources, we conclude that SHF played a dominant role in the HS heat content change during winter, while the effect of positive heat advection of the HWC can account for at least 29% of the HS heat content change. The immediately increased SST in the HWC region in the HS against the strong wind and large surface cooling during the winter storm events further demonstrated that the HWC was a wind-driven current. Since the monsoonal wind will be decreased in the future climate due to global warming (Kitoh, 2006), a lessened heat exchange between the HS and the open ocean may result from a weakening HWC during wintertime.

Acknowledgements

We thank the INGV, Italy for providing the ECMWF wind and SHF data. Qiao Lulu was supported by the China Scholarship Council for a seven-month study visit to the UNSW@ADFA in Australia. We aslo thank the Second Institute Oceanography for their support to Dr. Wang Xiaohua. We are grateful to two anonymous reviewers for their constructive reviews which have significantly improved the paper.

References

Blumberg A F. 1996. An estuarine and coastal ocean version of POM. Proceedings of the Princeton Ocean Model Users Meeting, Princeton, NJ

Chen S J, He W H, Yao S Y, et al. 1992. Definition of ocean and climatic season in the coastal sea of China. Acta Oceanologica Sinica, 14(6): 1–11

Csanady G T. 1981. Circulation in the coastal ocean. Adv Geophys, 23: 101–183

Guan B X. 1994. Patterns and structures of the currents

in Bohai, Huanghai and East China Seas. Oceanology of China Seas (in Chinese), 1: 17–26

Guo B H. 1993. Major Features of the Physical Oceanography in the Yellow Sea. Chineses Science Bulletin (in Chinese), 11(3): 7–18

Guo B H, Zou E M, Xiong X J, et a1. 2000. The seasonal variabilities of the sea water exchange between the Yellow Sea and the East China Sea. Acta Oceanologica Sinica, 22(Supp1): 13–23

Harney R. 1971. Surface thermal boundary condition for ocean circulation models. J Phys Oceanogr, 1: 241–248

Hsueh Y, Romea R D, De W, et al. 1986. Wintertime winds and coastal sea level fluctuations in the northeast China Sea: Part 2. Numerical model. J Phys Oceano, 16(2): 241–261

Huang D J, Fan X P, Tong D X, et al. 2005. Westward shift of the Yellow Sea warm salty tongue. Geophysical Research Letter, 32: L24613, doi:10.1029/2005GL024749

Josey S A, Kent E C, Tayor P K. 1998. The Southampton OceanographyCentre (SOC) Ocean-atmosphere Heat, Momentum and Freshwater Flux Atlas. Southampton, UK: Southampton Oceanography Centre, Report, 6: 1–33

Kitoh A. 2006. Asian monsoons in the future. In: Wang B, ed. The Asian Monsoon. Berlin: Springe, 631–649

Le K T, Mao H L. 1990. Wintertime structures of temperature and salinity of the southern Huanghai (Yellow) Sea and its current systems. Oceanologia et Limnologia Sinica (in Chinese), 21(6): 505–515

Lick W, Xu Y, McNeil J. 1995. Resuspension properties of sediments from the Fox, Saginaw, and Buffalo Rivers. Journal of Great Lakes Research, 21(2): 257–274

Liu X Q. 1996. Numerical simulation of the Yellow Sea wintertime circulation. Oceanologia et Limnologia Sinica (in Chinese), 27(5): 546–555

Ma J, Qiao F L, Xia C S, et al. 2006. Effects of the Yellow Sea Warm Current on the winter temperature distribution in a numerical model. J Geophy Res, 111: C11S04, doi:10.1029/2005JC003171

Nitani H. 1972. Beginning of the Kuroshio. In: Stommel H, Yoshida K, eds. Kuroshio, Physical Aspects of the Japan Current. Seattle: University of Wash Press, 129–156

Qiao L L. 2008. Circulation and sediments transport due to winter storms in the Bohai Sea and Yellow Sea (in Chinese): [dissertation]. Qingdao: Ocean University of China, 106

Riedlinger S K, Jacobs G A. 2000. Study of the dynamics wind-driven transports into the Yellow Sea during winter. J Geophys Res, 105(C12): 28695–28708

Tang Y X, Zou E M, Lie H J. 2001. On the origin and path of the Huanghai Warm Current during winter and early spring. Acta Oceanologica Sinica, 23(1): 1–12

Teague W J, Jacobs G A. 2000. Current observations on the development of the Yellow Sea Warm Current. J Geophys Res, 105(C2): 3401–3411

Uda M. 1936. The results of simultaneous oceanographical investigations in the Japan Sea and its adjacent waters during October and November, 1933. J Imp Fish Ecrp St, 7: 91–151

Wang J, Yuan Y. 1988. Numerical modeling of wintertime circulation in the East China Sea. Chinese J Oceano Limno, 6(4): 300–319

Wang X H, Symonds G. 1999. Coastal embayment circulation due to atmospheric cooling. J Geophys Res, 104: 29801–29816

Wang X H. 2005. Circulation of the northern Adriatic Sea (Italy) due to a Bora event in January 2001: a numerical model study. Ocean modeling, 10: 253–271

Xie S P, Hafner J, Tanimoto Y, et al. 2002. Bathymetric effect on the winter sea surface temperature and climate of the Yellow and East China Seas. Geophysical Research Letters, 29(24): doi: 10.1029/2002GL015884

Yu L, Jin X, Weller R A. 2008. Multidecade global flux datasets from the objectively analyzed air-sea fluxes (OAFlux) project: latent and sensible heat fluxes, ocean evaporation, and related surface meteorological variables. OAFlux Project Technical Report, OA-2008-01. Woods Hole, Massachusetts: Woods Hole Oceanographic Institution, 1–64

Yuan Y L, Guo B H, Sun X P. 1993. Physical oceanography in Pan-Yellow Sea Region. Chineses Science Bulletin (in Chinese), 11(3): 1–6

Zang J Y, Tang Y X, Zou E M, et al. 2001. Analysis of Yellow Sea circulation. Chineses Science Bulletin (in Chinese), 46(Suppl): 7–15